Investigations of radiation pressure : optical side-band cooling of a trampoline resonator and the effect of superconductivity on the Casimir force

Eerkens, H.J.

Cover Page

Universiteit Leiden

The following handle holds various files of this Leiden University dissertation:
http://hdl.handle.net/1887/59506

Author: Eerkens, H.J.
Title: Investigations of radiation pressure : optical side-band cooling of a trampoline resonator and the effect of superconductivity on the Casimir force
Issue Date: 2017-12-21

PART II

Casimir effect

<div style="text-align: right">*5*</div>

Thermal Casimir Force and Superconductors

The van der Waals force is carried by virtual photons that are exchanged by two interacting atoms or molecules. As their separation increases, the interaction is no longer instantaneous due to the finite speed of light. The result is a faster decay of the force with distance. Two macroscopic conducting plates at small separation are attracted to each other by the van der Waals interactions of the individual atoms, although the interactions cannot simply be added pairwise and one has to correct for the presence of the other atoms. When the plate separation becomes larger, one has to account again for the retardation of the interaction photons. This retarded van der Waals force between macroscopic bodies is better known as the Casimir force. The retarded van der Waals force is one interpretation of the origin of the Casimir force and several other methods exist to calculate this force [36]. One of these methods will be explored in this chapter..

In 1948, Hendrik Casimir calculated the interaction between two parallel plates due to the existence of the vacuum fluctuations of the electromagnetic field [37]. In his approach he considered perfectly reflecting, uncharged and nonmagnetic plates, having a reflectivity equal to one at all frequencies. Lifshitz later found that for real materials the force is determined by the values of the complex dielectric constant of the media involved [97]. However, one needs to know these values at all frequencies to compute the force. And this poses problems, since experimental characterization of the material is currently only accessible at certain frequency ranges. Extrapolating the data to all frequencies is possible via two different models. One model, the Drude model, accounts for frictional dissipation in the material, while in the other model, the plasma model, dissipation is not included. At room temperature, the difference appears only at the DC contribution to the Casimir force. To this day there remains controversy on which model is more appropriate.

Although the Casimir force is determined by the dielectric permittivity at all frequencies, not all frequency ranges contribute equally. It is possible to set the measurement conditions in a way that especially the low frequencies contribute, such

---

This chapter is written in collaboration with Francesco Intravaia.

that the difference between the models is most distinct. One solution is to measure the Casimir force at larger distances [50]. However, these measurements seem to conflict with precision measurements at smaller distances [11]. So measurements of this type have not given a decisive answer yet. Another solution is to measure the Casimir force at higher temperatures, but this is limited by experimental requirements, such as the maximum working temperature of piezo-electric transducers.

The solution we will explore is the use of superconducting materials [49]. Superconductors repel a static magnetic field due to the Meissner effect. Below the critical temperature, the contribution of this field to the total Casimir force is therefore known and can be used as a reference when the material is brought into a non-superconducting state.

In this chapter we will give the theoretical background of the Casimir force between real conductors. Since accurate derivations can be found in literature [36, 97, 98], we will only outline the main steps and focus on the important components. The influence of the models is shown and how the difference becomes apparent at larger distances and higher temperature. Finally we will introduce a simple model for the Casimir force between superconductors

5.1   Casimir force between perfect conductors

There are several ways to find an expression for the Casimir force between two parallel plates [36, 98–101]. Some of these methods calculate the electromagnetic modes that can exist between the plates and assign to each mode a zero-point energy $E_0 = \frac{1}{2}\hbar\omega$, with $\hbar$ the reduced Planck constant and $\omega = ck$ the angular frequency of the mode, with c the speed of light and k the wave vector. The total Casimir energy of the system can then be approached as the sum over all modes between the plates, minus the continuum of modes outside the plates:

$$E_C = \sum_\omega \frac{1}{2}\hbar\omega - \int \frac{\hbar c}{2}k \, \mathrm{d}k. \tag{5.1}$$

At first glance, this seems to result in an infinite energy. It is however reasonable to set a cut-off frequency that corresponds to a wavelength smaller than the size of the atoms of the plates. For waves at these frequencies, the plates form no obstacle and their zero-point energy is not influenced.

In his original paper [37] Casimir assumed that the plates are made of perfect conductors. Perfect conductivity means that the reflection coefficient of the plates is equal to plus or minus one (depending on the polarization). The possible waves in the direction normal to the plates therefore have wave numbers $k_z = \frac{\pi}{d}n_z$, with d the plate separation. For infinite plates the parallel wave vectors, k_x and k_y, are continuous, and so is k_z when the plate separation is infinite. Casimir calculated the energy difference between plates at infinite and finite separation and derived from that the following expression for the force per area A

$$F_C = -\frac{\pi^2 \hbar c A}{240 d^4}. \tag{5.2}$$

An interpretation of this force is that the discrete number of modes between the plates exert less radiation pressure than the continuous spectrum of modes outside the plates.

5.2 Lifshitz theory for the force between real conductors

The calculations to obtain the Casimir force become more elaborated when we no longer assume perfect reflectors. In this section we will outline the steps followed by Lifshitz to find an expression for the Casimir force. We will comment on its limitations and how they can be circumvented.

For real conductors, the boundary conditions of the plates are related to the complex dielectric permittivity

$$\varepsilon(\omega) = \varepsilon'(\omega) + i\varepsilon''(\omega), \tag{5.3}$$

where $\varepsilon'(\omega)$ accounts for the dispersion in the material and $\varepsilon''(\omega)$ for the absorption.

Furthermore, at finite temperatures T, the interacting photons have a distribution not only given by the zero-point fluctuations, but also by their Bose-Einstein statistics, with the number of photons in a mode with frequency ω given by

$$n(\omega) = \frac{1}{2} + \frac{1}{e^{\hbar\omega/k_BT} - 1} = \frac{1}{2}\coth\frac{\hbar\omega}{2k_BT}, \tag{5.4}$$

with k_B Boltzmann's constant. Note that the presence of these finite temperature fluctuations is directly linked to the absorption term $\varepsilon''(\omega)$ in the dielectric permittivity by the fluctuation-dissipation theorem. Absorption of radiation in the plates transforms the radiation energy into heat, which in turn causes thermal fluctuations in the plates.

Consider now two half spaces filled with two media (representing the parallel plates) separated by a distance d. This situation is depicted in Figure 5.1, where we have indicated the dielectric permittivities of the media with ε_1 and ε_2, these materials are taken to be nonmagnetic. Since in our measurements the space between the two plates is vacuum, we set $\varepsilon_3 = 1$. It is of course possible to extend the calculations by filling this space with some other medium (gas or fluid), which would alter the strength of the Casimir force, or even change its sign from attractive to repulsive [102–104].
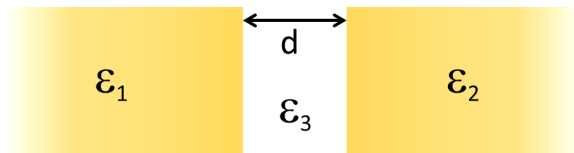

Figure 5.1: The parallel plates can be represented as two half spaces filled with media 1 and 2, separated by a distance d. The space in between (medium 3) is vacuum.

The force is derived [97] from the electric and magnetic fields between the plates, which in turn can be found by solving Maxwell's equations with the appropriate boundary conditions. For monochromatic electric and magnetic fields, in the form $\mathbf{E}_0 e^{-\mathrm{i}\omega t}$ and $\mathbf{B}_0 e^{-\mathrm{i}\omega t}$, we seek solutions of

$$\nabla \times \mathbf{E}_0 = \mathrm{i}\frac{\omega}{c}\mathbf{B}_0, \tag{5.5}$$

$$\nabla \times \mathbf{B}_0 = -\mathrm{i}\frac{\omega}{c}\varepsilon(\omega)\mathbf{E}_0 - \mathrm{i}\frac{\omega}{c}\mathbf{K}. \tag{5.6}$$

An extra fluctuating, random field $\mathbf{K}$ is added to account for the thermal and quantum fluctuations of the material's microscopic constituents [97, 105], and determined by its correlation function

$$\langle K_i(\mathbf{r})K_j(\mathbf{r}')\rangle = 2\hbar \coth\left(\frac{\hbar\omega}{2k_BT}\right)\varepsilon''(\omega)\delta_{ij}\delta(\mathbf{r}-\mathbf{r}'), \tag{5.7}$$

where the use of the δ-function means that the fluctuations are only locally correlated. We assume nonmagnetic materials, therefore only electric noise is added. This additional random field $\mathbf{K}$ is zero in the vacuum between the plates.

Solutions of Maxwell's equations are found in the two media and in the vacuum between them after demanding continuity of the normal and tangential components of the fields and transversality of the waves. These solutions are given in momentum space in terms of the wave vector $\mathbf{k}$, where we separate the component perpendicular to the plane of the gap $\mathbf{k}_z$ from the tangential components $\mathbf{k}_\parallel$ such that $k^2 = k_\parallel^2 + k_z^2$.

The Casimir force is derived from the zz-component of the Maxwell stress tensor, based only on the electric and magnetic fields in the vacuum between the plates. The fields in the plates still have influence on the force, because they shape the vacuum fields via the continuity conditions. The calculated fields are monochromatic, so the total force is obtained after an integration over all frequencies ω. The expressions for the fields contain another integration, over the tangential wave vector component $\mathbf{k}_\parallel$. To make the final expression more compact, this integration is transformed to an integration over a parameter p defined as

$$p = \sqrt{1 - \frac{c^2}{\omega^2}k_\parallel^2}. \tag{5.8}$$

The paths of integration for both p and ω are shown in Figure 5.2(a). The integration over ω is purely over the real axis, but the path of integration for p lies both on the real and imaginary axis, due to the integration over $k_\parallel$ from zero to infinity. This means that part of the integration is along a path where both p and ω are real. This is problematic because the integrand contains an expression $e^{-2\mathrm{i}p\omega d/c}$, which oscillates along this part, especially at large distances d. This can be solved by transforming the paths of integration via contour integration. Note that part of the contour is a semicircle with infinite radius, which does not depend on distance such that the contribution along this path goes to zero. The new paths of integration are depicted in Figure 5.2(b). The variable p is now purely real, but the frequencies ω have become purely imaginary.
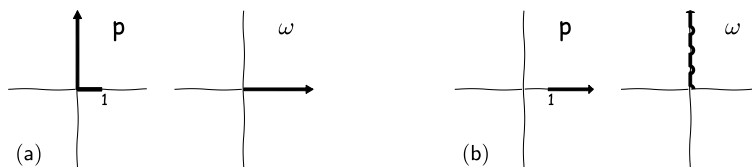
Figure 5.2: Integration paths for the integrals in the expression of the Casimir force: (a) As originally calculated, the integrand becomes highly oscillatory at the real part of the path of integration for p; (b) After transformation of the integration paths, the integrand no longer oscillates but the integration over ω is now over purely imaginary values.

At zero temperature, we can then replace $\omega = \mathrm{i}\xi$, with ξ real. At finite temperature, however, the integrand contains a term $\coth(\hbar\omega/2k_BT)$, which has poles along the imaginary frequency axis. According to Cauchy's residue theorem, the integral over the imaginary frequencies can be replaced by a sum over the residues at the poles. These poles are positioned at points where the argument of the cotangent is equal to a multiple of pi, so at frequencies

$$\omega_n = \mathrm{i}\xi_n = \mathrm{i}\frac{2\pi k_B T}{\hbar}n, \tag{5.9}$$

with n an integer. These frequencies are known as the Matsubara frequencies. Note that because of the residue theorem only these frequencies contribute to the force.

The total force per unit area is therefore described by a sum over these Matsubara frequencies and an integral over the parameter p, which represents the tangential wave vector component:

$$P_C = -\frac{k_B T}{\pi c^3} \sum_{n=0}^{\infty}{}' \int_1^{\infty} p^2 \xi_n^3 \left\{ \left[\frac{(s_1 + p)(s_2 + p)}{(s_1 - p)(s_2 - p)} e^{2p\xi_n d/c} - 1 \right]^{-1} \right.$$

$$\left. + \left[\frac{(s_1 + \varepsilon_1 p)(s_2 + \varepsilon_2 p)}{(s_1 - \varepsilon_1 p)(s_2 - \varepsilon_2 p)} e^{2p\xi_n d/c} - 1 \right]^{-1} \right\} \mathrm{d}p, \tag{5.10}$$

where $\varepsilon_j = \varepsilon_j(\mathrm{i}\xi_n)$ and where the parameter $s_j = \sqrt{\varepsilon_j(\mathrm{i}\xi_n) - 1 + p^2}$, with $j = 1, 2$, is introduced for compactness. The prime on the summation mark indicates that the $n = 0$ term is multiplied with an extra factor $\frac{1}{2}$. At zero frequency only half the residue is taken into the summation. Physically, this can be understood since zero-order modes only have one polarization while higher order modes have two polarizations.

This expression describes the Casimir force between two media 1 and 2 at nonzero temperature and holds for nonmagnetic media. For magnetic materials, the force can be derived with the magnetic permeability $\mu(\omega)$ included [102, 106, 107]. We will only consider nonmagnetic materials in this thesis. For spatially dispersive media, like superconductors, there is interaction among different parts of the system with a response that depends on their separation $\mathbf{r} - \mathbf{r}'$. In this situation the dielectric

permittivity is also influenced by contributions at this separation and depends, after a Fourier transform, on the wave vector: $\varepsilon = \varepsilon(\mathbf{k}, \omega)$ [108]. Note that the presence of the gap violates the translational invariance in the direction perpendicular to the plates required for the Fourier transform. It is therefore only a phenomenological approach to repeat the calculations leading to the Lifshitz expression while including the wave vector dependence [109], another possibility is to directly rewrite Eq. 5.10 in terms of the reflection coefficients of the plates [110]. If the parameters p and $s_{1,2}$ are written out, it is possible to recognize the Fresnel equations in Eq. 5.10. The full calculation is shown in Appendix A and leads to

$$P_C = -\frac{k_B T}{\pi} \sum_{n=0}^{\infty}{}' \int_0^{\infty} q_n k_{\parallel} \left\{ \left[\left(r_{\text{TE}}^{(1)} r_{\text{TE}}^{(2)} \right)^{-1} e^{2q_n d} - 1 \right]^{-1} \right.$$
$$\left. + \left[\left(r_{\text{TM}}^{(1)} r_{\text{TM}}^{(2)} \right)^{-1} e^{2q_n d} - 1 \right]^{-1} \right\} \mathrm{d}k_{\parallel}, \qquad (5.11)$$

where $q_n^2 = \frac{\xi_n^2}{c^2} + k_{\parallel}^2$ and $r_{\text{TE}}^{(1,2)}$ and $r_{\text{TM}}^{(1,2)}$ denote the reflection coefficients for the transverse electric and transverse magnetic modes respectively, the superscript indicates the corresponding medium. When the appropriate reflection coefficients are used, this equation for the Casimir force can also be used for spatially dispersive media.

5.3   Models for the dielectric permittivity

The Casimir force is determined by the reflectivity of the surfaces, which in turn depends on the dielectric permittivity of the materials. However, due to the transformation described in the previous section, the dielectric permittivity needs to be expressed in terms of imaginary frequencies. This expression is obtained via the Kramers-Kronig relation

$$\varepsilon(\mathrm{i}\xi) = 1 + \frac{2}{\pi} \int_0^{\infty} \frac{\omega \varepsilon''(\omega)}{\omega^2 + \xi^2} \mathrm{d}\omega. \qquad (5.12)$$

The integration over all real frequencies means that full knowledge of the dielectric permittivity is necessary to compare experimental data with theoretical calculations. For high frequencies, such data can be obtained from optical measurements and tabulated optical data are available for several materials[1] [112]. For the low frequency range where the dielectric permittivity is not determined experimentally, the data has to be extrapolated. One model that can be used for extrapolation [113, 114] is the Drude model for electrical conduction [115, 116]:

$$\varepsilon_D(\omega) = 1 - \frac{\Omega_p^2}{\omega(\omega + \mathrm{i}\gamma)}, \qquad (5.13)$$

---

[1]Note that the dielectric function depends on the sample preparation and therefore the best agreement between theory and experiment is achieved when the optical data is obtained from the actual sample that is used for the Casimir force measurements [111].

where Ω_p is the plasma frequency, which is given by

$$\Omega_p^2 = \frac{4\pi n_e e^2}{m^*} \tag{5.14}$$

with n_e the electron density, e the electron charge and m^* the effective mass of the electrons, and where γ is the relaxation frequency that accounts for Ohmic conductivity

$$\gamma = \frac{\Omega_p^2 \varepsilon_0}{\sigma_0}, \tag{5.15}$$

with σ_0 the static conductivity. It is therefore possible to obtain values for Ω_p and γ from measurements of the resistance in the material. The dielectric permittivity at imaginary frequencies according to the Drude model is given by

$$\varepsilon_D(\mathrm{i}\xi) = 1 + \frac{\Omega_p^2}{\xi(\xi + \gamma)}, \tag{5.16}$$

which can be used if no extensive optical data are available. However, due to some theoretical discrepancies that have been argued, but also refuted [48, 117–123], some prefer to use the plasma model of infrared optics:

$$\varepsilon_p(\omega) = 1 - \frac{\Omega_p^2}{\omega^2}. \tag{5.17}$$

In this model the dielectric permittivity is purely real, therefore the model does not account for Ohmic dissipation. This is contradictory with the fact that metals are resistive at low frequencies and the use of the plasma model would seem incorrect, except that certain Casimir force experiments have shown better agreement with this model than with the Drude model [11, 52, 107, 124]. Since the plasma model is purely real, using it to extrapolate the imaginary dielectric permittivity is not feasible. A solution is to use the plasma model at imaginary frequencies,

$$\varepsilon_p(\mathrm{i}\xi) = 1 + \frac{\Omega_p^2}{\xi^2}, \tag{5.18}$$

but this does not take the measured optical data into account. Optical spectra of real materials often contain extra resonances that are not modeled by the Drude and plasma models. These extra resonances are a result of a restoring force binding the core electrons to the nuclei [116]. To describe the optical spectrum including these resonances, the Drude model for metals is extended with Lorentz oscillators to the Drude-Lorentz model

$$\epsilon_{\mathrm{DL}}(\omega) = 1 - \frac{\Omega_p^2}{\omega(\omega + \mathrm{i}\gamma)} + \sum_j \frac{f_j}{\omega_{0j}^2 - \omega^2 - \mathrm{i}\beta_j\omega}, \tag{5.19}$$

where each oscillator j is described by an oscillator strength f_j, oscillator frequency ω_{0j} and damping rate β_j. Values for these parameters are obtained from fits to the

optical spectra. The dielectric permittivity at imaginary frequencies is more correctly described by the Drude-Lorentz model

$$\varepsilon_{\mathrm{DL}}(\mathrm{i}\xi) = 1 + \frac{\Omega_p^2}{\xi(\xi + \gamma)} + \sum_j \frac{f_j}{\omega_{0j}^2 + \xi^2 + \beta_j \xi},$$ (5.20)

or by the generalized plasma model [98]

$$\varepsilon_{\mathrm{gp}}(\mathrm{i}\xi) = 1 + \frac{\Omega_p^2}{\xi^2} + \sum_j \frac{f_j}{\omega_{0j}^2 + \xi^2 + \beta_j \xi}.$$ (5.21)

These models do account correctly for the resonances in the material, although resonances lying outside the range of the optical reflection measurements are not taken into account. In principle, the transformation of the optical data extrapolated via the Drude model to imaginary frequencies should result in the same dielectric permittivity as described by the Drude-Lorentz model. Note that by maintaining the resonances but setting $\gamma = 0$, the generalized plasma model does describe the relaxation of the core electrons, but not of the conduction electrons [98]. For the calculations presented in this chapter we use these Drude-Lorentz and generalized plasma models, although we may refer to them as the Drude and plasma models for simplicity.

To this day a controversy exists how to deal with the low frequency range of the dielectric permittivity. Both models can be used to calculate the Casimir force, such that comparison to precision measurements can give more insight in this issue. Figure 5.3 indicates how the dielectric permittivity of gold depends on the imaginary frequency ξ. Optical data are available [112] for frequencies higher than 1.9×10^{14} rad/s, for lower frequencies the dielectric permittivity is computed according to the Drude-Lorentz and generalized plasma models and the values $\Omega_p = 9.0$ eV and $\gamma = 35$ meV [114]. The deviation between the two models is clearly visible.

At finite temperature, the Casimir force is computed only at a finite set of frequencies, the Matsubara frequencies, since the contribution at other frequencies goes to zero[2]. It turns out that at room temperature, all except the zero-order frequency lie above 1.9×10^{14} rad/s, the lowest frequency at which optical data is available, the position of $\xi_1 = 2.4 \times 10^{14}$ rad/s is indicated in Figure 5.3. This means that the contribution of these frequencies can not reveal a difference between the Drude and plasma models. The difference only shows up in the zero-order Matsubara frequency, which represents a static field. Because the expressions for the dielectric permittivities diverge at zero frequency, we will continue our discussion in terms of the reflection coefficients mentioned in Eq. 5.11. The reflection coefficients are different for the TM and TE modes, which, at zero frequency, represent a static electric and static magnetic field respectively. The reflection coefficient can be determined by substituting the dielectric permittivities into the Fresnel equations (the expressions are given in Appendix A). For the zeroth order TM mode, which has only electric fields in the direction of propagation, the reflection coefficient becomes

$$r_{\mathrm{TM}}^{(D,p)}(\xi_0) = 1.$$ (5.22)

---

[2]Although the theory is developed at finite temperature, it is important to note that the problem how to extrapolate the dielectric permittivity to lower frequencies is not temperature dependent and also occurs at zero temperature.
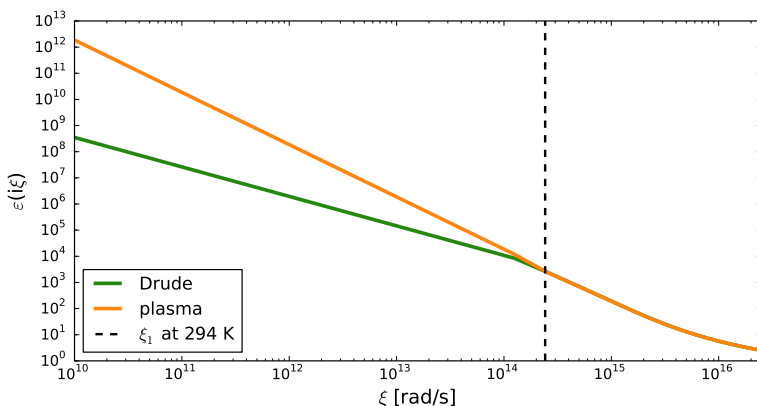
Figure 5.3: Dielectric permittivity of gold at imaginary frequencies $i\xi$ as a function of ξ. For frequencies above 1.9×10^{14} rad/s optical data are available, the extrapolation to lower frequencies was obtained with the values $\Omega_p = 9.0$ eV and $\gamma = 0.035$ eV. It is clear that the Drude and plasma models deviate at lower frequencies. The first order Matsubara frequency at room temperature is also indicated.

Note that this does not depend on the material and is also independent of temperature. More importantly, both Drude and plasma models predict the same coefficient. Physically, this value also makes sense, since metals reflect static electric fields.

The remaining term is the reflection coefficient of the static magnetic field, the zeroth order TE mode. This does have a different value for each model. The Drude model predicts

$$r_{\text{TE}}^{(D)}(\xi_0) = 0, \tag{5.23}$$

which physically can be understood since nonmagnetic materials form no obstacles for static magnetic fields. When substituted into the Lifshitz expression, this term results in a zero contribution to the Casimir force. This value is independent of Ω_p and γ and is purely a consequence of this model. According to the Drude model, therefore, only the static electric term contributes to the force at zero frequency.

The plasma model predicts a different coefficient:

$$r_{\text{TE}}^{(p)}(\xi_0) = \frac{k_\parallel c - \sqrt{k_\parallel^2 c^2 + \Omega_p^2}}{k_\parallel c + \sqrt{k_\parallel^2 c^2 + \Omega_p^2}}. \tag{5.24}$$

This leads to a nonzero contribution to the Casimir force, which is somewhat smaller than the contribution of the zeroth order TM mode. For large distances, $d \gg \frac{c}{2\Omega_p}$, and large temperatures the contribution approximates to the value at the zeroth order TM mode, which makes the total zeroth order contribution of the plasma model twice as large as the Drude model in this limit.

5.4   The effect of the different models on the Casimir force

Since a controversy exists on how to deal with the low frequency contribution of the dielectric permittivity to the Casimir force, experimental data are necessary to give a final verdict. Since only the zeroth order TE mode differs for both models, it is important to minimize the effect of the higher order modes. If we take a closer look at Eq. 5.11, we notice the factors

$$e^{-2q_n d} = e^{-2\sqrt{\xi_n^2/c^2+k_\parallel^2}\,d}. \tag{5.25}$$

The result of this term is that the Casimir force quickly reduces with distance and with ξ_n. Recall that the Casimir force is a sum of the contributions at the Matsubara frequencies. For larger distances, less Matsubara frequencies contribute to the force. This influence is visualized in Figure 5.4. The Casimir pressure as a function of distance, for two gold coated plates at room temperature, is shown in Figure 5.4(a). The difference between the two models only becomes visible at distances approaching $1\,\mu m$ or larger. The Matsubara frequencies that contribute to the force are shown in Figures 5.4(b) and 5.4(c), for a distance of $100\,nm$ and $1\,\mu m$ respectively. Note that the contributions of both models overlap for the frequencies ξ_n with $n > 0$. At a distance of $100\,nm$, many frequencies have to be considered, whereas at $1\,\mu m$ only the input of the first couple of frequencies is significant. Therefore, the relative contribution of the zeroth order Matsubara frequency is larger and the effect of the zeroth order TE mode is more likely to be detected.
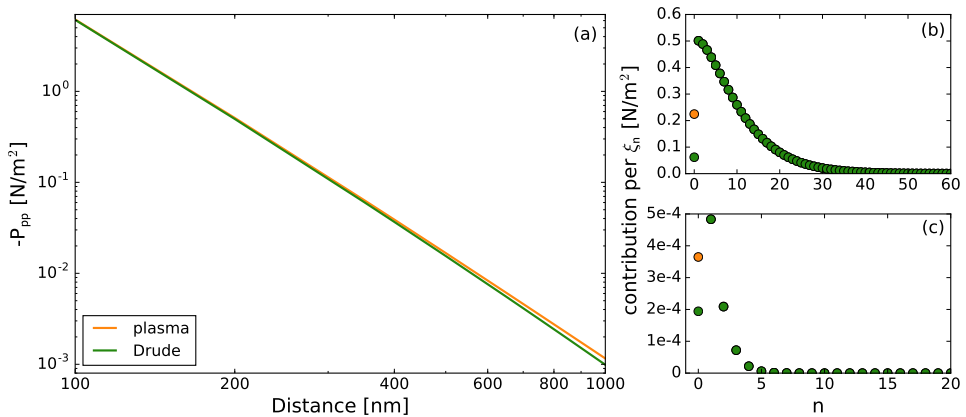

Figure 5.4: Distance dependence: (a) Casimir pressure as a function of distance at room temperature, the two models give diverging contributions only at larger distances; (b) Contribution of the different Matsubara frequencies for the two models at a distance of $100\,nm$; (c) At a distance of $1\,\mu m$ less Matsubara frequencies contribute to the force.

There is a lot of interest to resolve the difference between the models via precise

measurements at large distances [11, 47, 50, 98]. But since the Casimir force reduces rapidly with distance, the signal quickly becomes too small to detect. So far, measurements of the distance dependence of the force have not resulted in a conclusive answer yet.

Another approach may be more successful. Since the Matsubara frequencies depend linearly on temperature, raising the temperature has a similar effect as increasing the distance without reducing the force. Measurements of the Casimir force at higher temperatures therefore should also show the difference between the two models [125]. In Figure 5.5(a) we have plotted the temperature dependence of the Casimir force for the two models. The distance between the plates is set at $100 \, \text{nm}$, where the force can easily be detected.

While evaluating the temperature dependence, we must be careful to note that not only the force itself is a function of temperature (due to the interacting thermal photons), but that also the dielectric permittivity as described by the Drude model changes with temperature. The relaxation frequency γ is temperature dependent because it is related to the conductance of the material. If no impurities are present, the material's resistivity can be described with the Bloch-Grüneisen formula, such that for gold [48]

$$\gamma(T) = 0.087 \left(\frac{T}{\Theta}\right)^5 \int\limits_0^{\Theta/T} \frac{x^5 e^x}{(e^x - 1)^2} \, \mathrm{d}x, \tag{5.26}$$

with $\Theta = 175 \, \text{K}$ the Debye temperature for gold. Of course, this is only a model. It would be better to use measurements of the dielectric permittivity of the material at all temperatures of interest. Since these data are only sporadically available, we have to revert to the model. The temperature-dependent dielectric permittivity is calculated using a plasma frequency of $\Omega_p = 9.0 \, \text{eV}$ and a relaxation frequency given by Eq. 5.26. Note that compared to the dielectric permittivity obtained from optical reflection measurements this model underestimates the permittivity at higher frequencies. For comparison, the graph in Figure 5.5(a) shows two calculations for the Drude model, one based on the optical data of gold with the relaxation frequency kept constant at the room temperature value of $35 \, \text{meV}$ (green line) and one with the permittivity calculated via the model only (yellow line). Note that since the model underestimates the permittivity, the Casimir force is also estimated lower than in reality. Without the availability of optical data at a large temperature range, we will continue our calculations with the temperature-independent relaxation frequency.

The relative difference between the two models, normalized to the plasma model, is shown in Figure 5.5(b). As expected, the difference increases with temperature. A significant difference, of more than a few percent, arises at temperatures above $1000 \, \text{K}$, which is technically unrealistic to achieve. This requirement can be relieved by using a combination of larger distance and a temperature lower than $1000 \, \text{K}$, but higher than room temperature. At a distance of $400 \, \text{nm}$, there is a significant difference of more than 10 percent at a temperature of $600 \, \text{K}$. The effect might also be investigated by varying the temperature over a large range. Figure 5.5(a) shows that in the plasma model, the Casimir force is monotonically increasing with temperature, while the Drude model predicts a slight decrease in a certain temperature
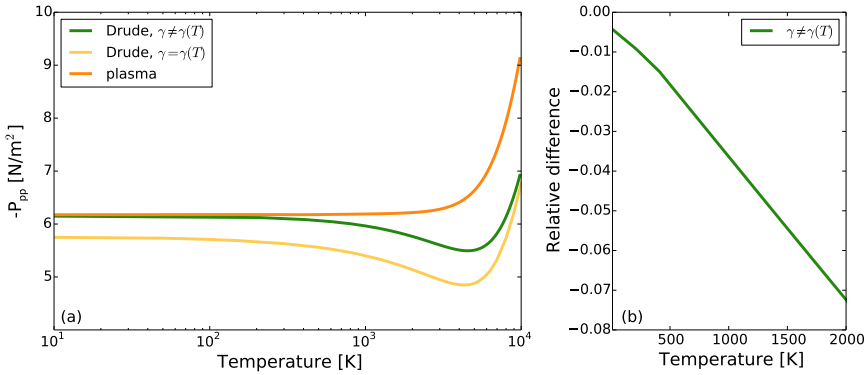
Figure 5.5: Temperature dependence of the Casimir force, for a distance of $100\,\text{nm}$ between the plates: (a) At higher temperatures the two models diverge. The green line shows the influence of the Drude model with γ kept at the room temperature value of $35\,\text{meV}$, while for the yellow line the relaxation rate is calculated according to Eq. 5.26; (b) Difference between the Drude and plasma models, normalized to the plasma model, for the temperature independent dielectric permittivity.

range. From a temperature scan at a fixed distance, the model can be deduced from the sign of the force's rate of change. This does, however, require a large achievable temperature range.

So, by increasing the distance or the temperature the influence of higher order Matsubara frequencies is decreased, and therefore the relative influence of the zeroth order modes is increased. This allows investigation of the effect of these terms at the cost of the necessity of very accurate measurements.

5.5 Casimir force between superconductors

There is another approach to specifically investigate the effect of the zeroth order TE mode. Recalling that this mode represents a static magnetic field, and that superconductors expel such a field, measuring the Casimir force between superconductors is a logical and more direct step to approach the issue [49, 55, 126]. A disadvantage of using superconductors is that measurements can only be performed at low temperatures, where the amount of higher order frequencies contributing to the force is increased significantly compared to room temperature. This lessens the relative effect of the zero-order frequency.

Just as with normal conductors, to calculate the Casimir force between superconductors full knowledge of the dielectric permittivity of the material is required. There are several models describing the conductivity of superconductors, from which the dielectric permittivity at imaginary frequencies can be deduced. Two of these models will be discussed below. Both models operate in the local limit, where the dielectric permittivity only depends on the frequency and not on the wave vector or on

position. A model for the dielectric permittivity in the non-local limit, which would be more correct for spatially dispersive superconductors, can be deduced from Ref. [127].

The macroscopic two-fluid model [128] describes superconductivity on the basics of thermodynamics. It states that only part of the conduction electrons contribute to the supercurrent, while the other conduction electrons remain normal. The core electrons remain unaltered, their contribution to the dielectric permittivity is described by the Lorentz oscillations. The superconducting electrons have no dissipation, so they are best described by the plasma model. For the normal electrons it is generally accepted that they are dissipative and can therefore be described by the Drude model. We will first follow this description, later in this section we will explain the results if we apply the plasma model description for the normal electrons as well. The ratio of superconducting electrons to normal electrons is temperature dependent and follows the Gorter-Casimir order parameter $\eta(T)$:

$$\eta(T) = \left[1 - \left(\frac{T}{T_c}\right)^4\right]\Theta(T_c - T), \tag{5.27}$$

$$\Theta(x) = \left\{ \begin{array}{ll} 0, & x < 0 \\ 1, & x \geqslant 0 \end{array} \right.$$

Above the critical temperature there are no superconducting electrons, which is ensured in the model by the Heaviside step function $\Theta(x)$. The conductivity of a superconductor, and therefore its dielectric permittivity, is a sum of the supercurrent permittivity and the permittivity of the normal electrons [129], with the Lorentz oscillators also included:

$$\epsilon_{2\mathrm{F}}(\mathrm{i}\xi) = 1 + \frac{\Omega_p^2}{\xi^2}\eta(T) + \frac{\Omega_p^2}{\xi(\xi + \gamma)}(1 - \eta(T)) + \sum_j \frac{f_j}{\omega_{0j}^2 + \xi^2 + \beta_j\xi}, \tag{5.28}$$

where Ω_p and γ are the plasma and relaxation frequencies of the superconducting material in the normal state. Note that due to the character of the order parameter, the permittivity behaves plasma-like at zero temperature and Drude-like close to the critical temperature. As the temperature decreases, more electrons contribute to the supercurrent and the system is less influenced by Ohmic dissipation. Since the two-fluid model assumes that the normal electrons in the superconductor are described by the Drude model, this assumption should be continued above the critical temperature in order to warrant a continuous transition across the critical temperature. The Casimir force gradually changes from the value predicted by the Drude model above the critical temperature to a value predicted by the plasma model as the temperature approaches $0\,\mathrm{K}$. For simplicity, we will call the combination of the two-fluid model for superconductors and the Drude model for the normal state, including the Lorentz oscillators, the Drude-two-fluid model.

In the plasma model description, the situation is different. The normal electrons above the critical temperature are described by the generalized plasma model. Below the critical temperature the resistivity of the normal electrons would not change, such that in the superconductor both the normal electrons and the superconducting

electrons follow the plasma model. The change in their ratio with temperature therefore does not alter the dielectric permittivity of the material and the superconducting transition has no effect at all on the Casimir force. In the following, we will refer to the two-fluid model combined with the generalized plasma model description for the normal electrons simply as the plasma model.

The absence or presence of an effect of the superconducting transition is directly measurable as the temperature is changed across the critical temperature. Since it is a relative measurement, it requires a less strict calibration of the set-up than with measurements at large distances. Compared to the high temperature measurements, it has the advantage of a relative small temperature change between $0\,\mathrm{K}$ and the critical temperature. In this chapter we will estimate the magnitude of the change in the Casimir force, measurements of the force will be discussed in chapter 8.

To arrive at an expression for the Casimir force, we can follow the same procedure as with normal conductors. The expression is given by Eq. 5.11, where the reflectivity of the superconductor is deduced via the Fresnel equations. The zero-order terms are based on a reflectivity of one for the TM mode for both the Drude-two-fluid model and the plasma model. As with normal conductors, the static electric field is repelled. The reflectivity of the zero order TE mode in the plasma model is the same as given by Eq. 5.24, in the Drude-two-fluid model we insert the two-fluid dielectric permittivity at imaginary frequencies in the Fresnel equations and then take the limit $\xi \to 0$, the resulting term is given by

$$r_{\mathrm{TE}}^{(2\mathrm{F})}(\xi_0) = \frac{k_\parallel - \sqrt{k_\parallel^2 + \eta(T)\Omega_p^2/c^2}}{k_\parallel + \sqrt{k_\parallel^2 + \eta(T)\Omega_p^2/c^2}}. \tag{5.29}$$

At $T = T_c$, this correctly leads to the Drude reflectivity $r_{\mathrm{TE}}^{(D)} = 0$, while at $T \ll T_c$ the plasma zero-order reflectivity is recovered. Note that for ideal metals ($\Omega_p \to \infty$) the plasma zero-order reflectivity goes to -1, i.e. perfect reflection of the static magnetic field due to the Meissner effect.

The two-fluid model is only a phenomenological model, a more complete description for superconductors is given by the microscopic BCS-theory [130, 131]. From the current density in a superconductor [132], it is possible to deduce the conductivity [133]:

$$\sigma(\omega) = -\mathrm{i}\frac{2n_e e^2 \gamma}{m^*\omega} \int\limits_{-\infty}^{\infty}\int\limits_{-\infty}^{\infty} \left\{ L(\omega, \epsilon, \epsilon') - \frac{f(\epsilon) - f(\epsilon')}{\epsilon' - \epsilon} \right\} \frac{1}{(\epsilon' - \epsilon)^2 + \gamma^2} \, \mathrm{d}\epsilon \, \mathrm{d}\epsilon' \tag{5.30}$$

where ϵ is the energy measured from the Fermi surface, $f(\epsilon)$ the Fermi-Dirac function and the spectral function $L(\omega, \epsilon, \epsilon')$ is a function of the quasi-particle energy $E = \sqrt{\epsilon^2 + \Delta(T)^2}$ and the BCS gap $\Delta(T)$. Note that the BCS theory also assumes dissipative normal electrons, and should therefore only be used in combination with the Drude model description. The integration over ϵ and ϵ' is computationally consuming, and via the Kramers-Kronig relations another integration over the frequency is needed to arrive at the desired expression of the dielectric permittivity at imaginary frequencies. A less consuming calculation is offered in Ref. [134]. There it was found

that impurity scattering lowers the dielectric permittivity and therefore the Casimir force compared to the two-fluid model. This means that according to BCS theory, at $T \ll T_c$ the Casimir force will not reach the value predicted by the plasma model. The calculations in this chapter, obtained with the two-fluid model, therefore give an overestimation of the Casimir force and therefore of the expected influence of superconductivity on the Casimir force.

The calculated Casimir pressure between two plates of niobium titanium nitride (NbTiN) is shown in Figure 5.6(a) as a function of temperature. NbTiN is the material we use in our experiments and has a critical temperature (T_c) of 13.6 K. In the calculations, the plates are separated by 100 nm. The Casimir pressure according to the plasma model is indicated by the orange line. The green line shows the Casimir pressure as calculated by the Drude-two-fluid model.
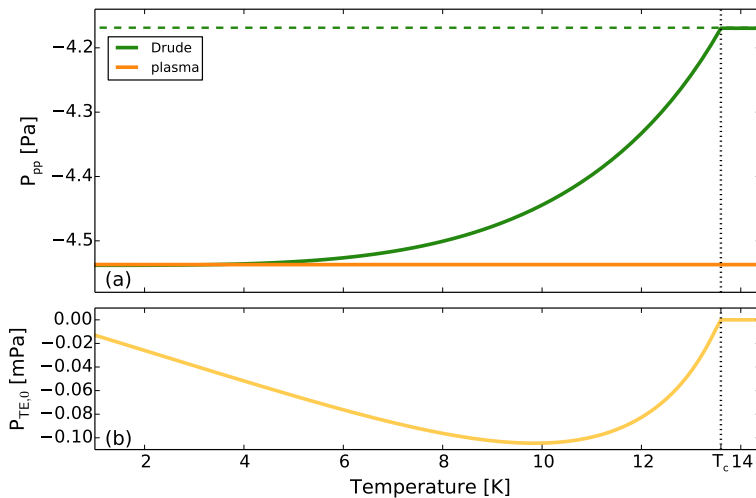

Figure 5.6: Casimir pressure between two niobium titanium nitride plates at a distance of 100 nm: (a) Total pressure described by the Drude model plus two-fluid model (green line) and plasma model (orange line). The Lorentz oscillations accounting for the core electrons are included in the calculations. According to the Drude model description, the pressure between the two superconductors transitions from the Drude model value above the critical value of 13.6 K towards the plasma value at 0 K. The plasma model description predicts no significant changes over temperature. The calculations are based on a plasma frequency of $\Omega_p = 5.33$ eV and relaxation rate $\gamma = 0.42$ eV; (b) Contribution of the zero order TE mode only, the calculation is based on the reflectivity given in Eq. 5.29.

Below the critical temperature, the magnitude of the pressure increases towards the pressure calculated by the plasma model. For comparison, the calculation based on the Drude model only is extended by the dashed green line below the critical temperature, as if no superconducting transition occurs. All the calculations are based on a plasma frequency of $\Omega_p = 5.33$ eV and relaxation frequency of $\gamma = 0.42$ eV. The contributions of four Lorentz oscillators are included as well. We refer to chapter 8

for a more detailed description of how these values are obtained from optical spectra of NbTiN.

As predicted, the plasma model shows no change with temperature. The Drude-two-fluid model shows a gradual transition in the Casimir pressure from the Drude model value above the critical temperature to the plasma model value at $T \ll T_c$. The superconducting transition should therefore only show a significant change in Casimir pressure with temperature for the Drude model. If we compare the expected Casimir pressure at low temperature with the pressure just above the critical temperature, we find a difference of 8.8% compared to the pressure around T_c. A temperature-dependent measurement of the Casimir force can therefore distinguish between the two models as the absence or presence of a change of the order of 8.8%, which should be detectable with our current measurement accuracy.

The contribution of the zero-order TE mode in the Drude-two-fluid model is plotted in Figure 5.6(b). Above the critical temperature it is equal to zero, as the Drude model describes. Below the critical temperature, the contribution increases as the reflectivity increases according to Eq. 5.29. Due to the prefactor $k_B T/\pi$ in Eq. 5.11, this zero-order contribution also decreases eventually as the temperature is decreased. Note that the zero-order contribution is very small compared to the total Casimir pressure, the change in this term is too small to explain the total effect of 8.8% change with temperature.
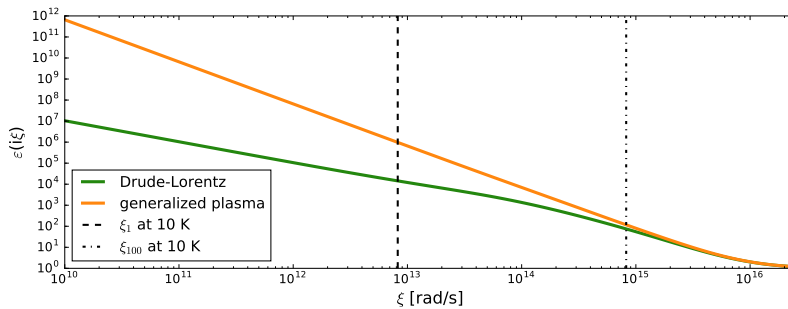

Figure 5.7: Dielectric permittivity of niobium titanium nitride at imaginary frequencies iξ as function of frequency. The plot is based on actual optical data of our NbTiN sample, extrapolated to lower frequencies either via the Drude-Lorentz model (green line) or generalized plasma model (orange line). The position of the first order Matsubara frequency at $10\,\mathrm{K}$ is indicated and shows that the two models predict different contributions at this frequency as well. Even at the hundredth Matsubara frequency, also indicated, the two models differ.

To better understand this seeming discrepancy, we take a closer look at the dielectric permittivity of niobium titanium nitride at imaginary frequencies, which is plotted in Figure 5.7. This plot is similar to the graph in Figure 5.3. In chapter 8 we will explain how the optical data were obtained that lead to values for the plasma and relaxation frequencies as well as the parameters describing the Lorentz oscillators, which are used either for the Drude-Lorentz model (green line) or for the

generalized plasma model (orange line).

Compared to the dielectric permittivity of gold, the two models coincide at a much higher frequency, this is caused by the higher resistivity of NbTiN (we measured a resistivity of $1.1 \pm 0.6 \times 10^{-6}\,\Omega\,\text{m}$, two orders of magnitude higher than reported values of gold). The vertical dashed line indicates the position of the first order Matsubara frequency at $10\,\text{K}$. Note that in contrast to the situation with gold, both models lead to a different dielectric permittivity at this frequency, which means that both models contribute differently to the Casimir force at this frequency. Even up to the hundredth Matsubara frequency, differences could be observed between the models. Although the total number of contributing Matsubara frequencies is larger at low temperatures (at $10\,\text{K}$, this is about 2500), there still are relatively more frequencies at which the contribution is different for the two models than in the case of gold at room temperature. These added contributions at the first hundred Matsubara frequencies can explain a much larger total difference in the Casimir force than can be explained by the zero-order TE mode only.

5.6   Casimir force with experimental parameters

The calculations so far are based on an idealized situation. In an experimental set-up, certain parameters differ from this situation, which may influence the effect of the superconducting transition. Although the calculations all express the Casimir force in the plate-plate geometry, actually measuring the force between two plates is technically challenging [135]. Most experiments, as well as the experiments in this thesis, are set up in a sphere-plate geometry. A theoretical prediction about the force between a sphere and a plate, can be derived from the parallel-plate pressure via the proximity force approximation (PFA) [136–138], which relates the parallel-plate pressure to the sphere-plate force gradient:

$$\frac{\partial F_{sp}}{\partial d} \approx 2\pi R P_{pp}, \tag{5.31}$$

where R is the sphere radius. The error in the approximation is estimated [139] to be of the order of d/R, which for significantly large spheres with a radius around $100\,\mu\text{m}$, at distances around $100\,\text{nm}$ is around a tenth of a percent. Since we are ultimately only interested in a relative difference below and above the critical temperature, this error falls away. In our experimental set-up we measure the sphere-plate force gradient divided by the sphere radius, which is equal to 2π times the parallel-plate pressure.

The choice of which superconductor to use is motivated by several arguments. As mentioned in section 5.4, less higher order Matsubara frequencies contribute to the force when the temperature increases. If we want to investigate specifically the effect of the 0-frequency contribution, we want to do the measurements preferably at a high temperature. Superconductors with a high critical temperature exist, but can be prone to oxidation, which may result in surface charges. These charges hinder the calibration of our set-up. We have therefore chosen niobium titanium nitride (NbTiN) as our superconductor. Thin film NbTiN has a critical temperature near $15\,\text{K}$ [140] and the presence of the nitrogen atoms prevents oxidation.
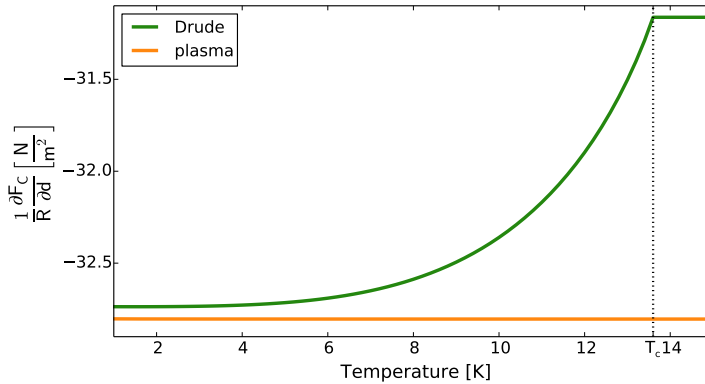
Figure 5.8: Casimir force gradient, normalized to the sphere radius, between a gold sphere and a niobium titanium nitride plate as a function of temperature. The green line shows the situation where the gold sphere and the normal electrons in the NbTiN plate are described by the Drude model, while the orange line shows a description by the plasma model.

During the measurements we want to be sure that the superconductors are indeed in the superconducting state. For the plate, this can be done by monitoring the plate's resistance. But for the sphere, this is technically more challenging since attaching wires to a microsphere is not very feasible. A more feasible method would be to position the sphere in a magnetic field and read out the change in this field by a SQUID as the sphere transitions to its superconducting state [141]. But this required a significant alteration to our initial set-up. We have therefore chosen to pair the superconducting plate with a gold sphere. Note that this is far from ideal if we wish to probe the zero-frequency term specifically. The Casimir force depends on the multiplication of the reflectivities of the surfaces. For the TE mode at zero frequency, the Drude model sets the reflectivity of gold to zero, such that the effect of the change in static reflectivity of the superconductor is canceled. Physically, it is like only one mirror exists for this mode. The plasma model does lead to nonzero contributions of both mirrors, but they are small and hard to distinguish in comparison to the zero contribution predicted by the Drude model. However, the higher order modes still lead to significant changes between the Drude and plasma models, so the effect of the superconducting transition should still be visible as a possible change in the contribution of these modes.

Figure 5.8 shows the Casimir force gradient, normalized to the sphere radius, between a gold coated sphere and a NbTiN plate as a function of temperature at a sphere-plate separation of $100\,\mathrm{nm}$.

Two situations are depicted. In the first situation (green line), the spherical gold surface and flat niobium titanium nitride surface above the critical temperature are described by the Drude-Lorentz model, while the superconductor (NbTiN below the critical temperature) follows the the two-fluid model. As with the parallel NbTiN plates, Figure 5.6, there is a continuous transition across the critical temperature. At

$T \ll T_c$, the force gradient does approach the plasma-model prediction, but does not reach the same value, since the gold sphere still follows the Drude-Lorentz model.

In the second situation, the gold surface follows the generalized plasma model, as does the NbTiN in its normal state. The two-fluid model is still used for the superconductor, but now describes a mixture of plasma-like superconducting electrons and plasma-like normal electrons, so in effect we can use the generalized plasma model for the NbTiN below the critical temperature as well. The orange line in Figure 5.8 indicates that there is hardly any change in the Casimir force gradient with temperature.

In the Drude model description, the force gradient changes about 5.1% compared to the value at the critical temperature. This is less than the change with temperature between two NbTiN parallel plates, but it is still measurable. For comparison, room temperature measurements were reported with a relative error of 0.19 to 9.0 percent [11].

5.7   Conclusions and outlook

The Casimir force between real conductors is determined by the frequency dependent, complex dielectric permittivity of the opposing surfaces. Full knowledge of the dielectric permittivity is required, since electromagnetic waves at all frequencies (up to a certain cut-off frequency) contribute. To avoid oscillations in the integrand, the frequency path of integration is transformed from real to imaginary frequencies. At finite temperatures, only a discrete set of frequencies, known as the Matsubara frequencies ξ_n, contribute to the Casimir force. The dielectric permittivity at a certain Matsubara frequency follows from a integration of the dielectric permittivity over all real frequencies, but the integrand is weighted by each ξ_n, such that the greatest contribution comes from the frequency range around the given Matsubara frequency. Effectively, only knowledge of the dielectric permittivity around the Matsubara frequencies is necessary, which somewhat lifts the requirement to know the full dielectric permittivity. For gold at room temperature, the dielectric permittivity at all higher order frequencies can be deduced from measurements and only the static contributions remain unknown. Since the contribution from the static electric field can be determined from the reflectivity, only the contribution from the static magnetic field remains open to debate. In superconductors, the reflectivity for the static magnetic field is determined by the Meissner effect. Therefore, measurements of the Casimir force between superconductors may give information on the contribution of this field to the total force.

For two plates of niobium titanium nitride, we calculate an effect of 8.8 percent across the superconducting transition. This is significantly larger than what you would expect based on a possible change at only one Matsubara frequency. From the dielectric permittivity of NbTiN at imaginary frequencies we can induce that certain higher order modes also contribute differently to the Casimir force for the Drude and plasma models. Across the superconducting transition it is not only the zero-order mode that changes, which explains the large effect. For an experimentally more accessible geometry of a niobium titanium nitride plate paired with a gold sphere, this

effect is smaller, a little more than 5 percent. Note that our calculations overestimate these percentages, since the two-fluid model predicts a larger effect than the physically more correct BCS theory. The experiments in the following chapters will show whether the effect of the superconducting transition is indeed measurable and if so, what the magnitude of this effect to the Casimir force is.